ANL-77-72

ANL-77-72

CYCLIC-DEFORMATION RESISTANCE OF WELD-DEPOSITED TYPE 16-8-2 STAINLESS STEEL AT 593°C

by

D. T. Raske

Does not contain Export Controlled information

Export Control Review Number 25647

Date of Review 4/22/2010

Reviewer Initials MKH

APPLIED TECHNOLOGY

Any further distribution by any holder of this document or of the data therein to third parties representing foreign interests, foreign governments, foreign companies and foreign subsidiaries or foreign divisions of U. S. companies should be coordinated with the Director, Division of Reactor Development and Demonstration, U. S. Energy Research and Development Administration.

U of C-AUA-USERDA

ARGONNE NATIONAL LABORATORY, ARGONNE, ILLINOIS

Prepared for the U. S. ENERGY RESEARCH AND DEVELOPMENT ADMINISTRATION under Contract W-31-109-Eng-38

Digitized 06/09/2008

ANL-77-72

ANL-77-72

CYCLIC-DEFORMATION RESISTANCE OF WELD-DEPOSITED TYPE 16-8-2 STAINLESS STEEL AT 593°C

by

D. T. Raske

APPLIED TECHNOLOGY

Any further distribution by any holder of this document or of the data therein to third parties representing foreign interests, foreign governments, foreign companies and foreign subsidiaries or foreign divisions of U. S. companies should be coordinated with the Director, Division of Reactor Development and Demonstration, U. S. Energy Research and Development Administration.

UWC-AUA-USERDA

ARGONNE NATIONAL LABORATORY, ARGONNE, ILLINOIS

Prepared for the U. S. ENERGY RESEARCH AND DEVELOPMENT ADMINISTRATION under Contract W-31-109-Eng-38

The facilities of Argonne National Laboratory are owned by the United States Government. Under the terms of a contract (W-31-109-Eng-38) between the U. S. Department of Energy, Argonne Universities Association and The University of Chicago, the University employs the staff and operates the Laboratory in accordance with policies and programs formulated, approved and reviewed by the Association.

MEMBERS OF ARGONNE UNIVERSITIES ASSOCIATION

The University of Arizona
Carnegie-Mellon University
Case Western Reserve University
The University of Chicago
University of Cincinnati
Illinois Institute of Technology
University of Illinois
Indiana University
Iowa State University
The University of Iowa
Kansas State University
The University of Kansas
Loyola University
Marquette University
Michigan State University
The University of Michigan
University of Minnesota
University of Missouri
Northwestern University
University of Notre Dame
The Ohio State University
Ohio University
The Pennsylvania State University
Purdue University
Saint Louis University
Southern Illinois University
The University of Texas at Austin
Washington University
Wayne State University
The University of Wisconsin

NOTICE

This report was prepared as an account of work sponsored by the United States Government. Neither the United States nor the United States Department of Energy, nor any of their employees, nor any of their contractors, subcontractors, or their employees, makes any warranty, express or implied, or assumes any legal liability or responsibility for the accuracy, completeness or usefulness of any information, apparatus, product or process disclosed, or represents that its use would not infringe privately-owned rights. Mention of commercial products, their manufacturers, or their suppliers in this publication does not imply or connote approval or disapproval of the product by Argonne National Laboratory or the U. S. Department of Energy.

Printed in the United States of America
Available from
U. S. Department of Energy
Technical Information Center
P. O. Box 62
Oak Ridge, Tennessee 37830
Price: Printed Copy $4.50

Distribution Category:
LMFBR Structural Materials and
Design Engineering (UC-79h)

ANL-77-72

ARGONNE NATIONAL LABORATORY
9700 South Cass Avenue
Argonne, Illinois 60439

CYCLIC-DEFORMATION RESISTANCE OF WELD-DEPOSITED TYPE 16-8-2 STAINLESS STEEL AT 593°C

by

D. T. Raske

Materials Science Division

August 1977

TABLE OF CONTENTS

	Page
ABSTRACT	7
I. INTRODUCTION	7
II. SCOPE	8
III. EXPERIMENTAL PROGRAM	8
A. Type 316 Stainless Steel Baseline Data	8
B. Materials and Specimens	8
C. Apparatus and Test Procedure	11
IV. RESULTS AND DISCUSSION	13
A. Continuous-cycling and Tension Hold-time Fatigue Tests	13
B. Initial Monotonic Tensile Data and Cycle-dependent Changes in Mechanical Properties	18
V. CONCLUSIONS	22
APPENDIX: Metallographic and Fractographic Analysis of Creep-fatigue and Creep-rupture Specimens	23
ACKNOWLEDGMENTS	33
REFERENCES	34

LIST OF FIGURES

No.	Title	Page
1.	Total Strain Range vs Cycles to Failure, Showing Effect of Tension Hold Time on Fatigue Life for Type 316 Stainless Steel Baseline Data	9
2.	Macrograph of Fusion Zone between Type 316 Stainless Steel Base Metal and ASA Type 16-8-2 Stainless Steel Weld Metal	9
3.	Distribution of Ferrite in ASA Type 16-8-2 Stainless Steel Weld Metal	9
4.	Microstructure of ASA Type 16-8-2 Stainless Steel Weld Metal	10
5.	Microstructure of Type 316 Stainless Steel	10
6.	ASA Type 16-8-2 Stainless Steel Weld-metal Test Specimens	11
7.	Liquid-metal Grip Showing a Specimen Surrounded by Induction-heating Coil and with Axial Extensometer Attached	12
8.	Total Strain Range vs Cycles to Failure for ASA Type 16-8-2 Stainless Steel Weld Metal Compared with Type 316 Stainless Steel Baseline Data	14
9.	Ranges of Total, Elastic, and Plastic Strain vs Cycles to Failure for ASA Type 16-8-2 Stainless Steel	15
10.	Total Strain Range vs Cycles to Failure for Types 16-8-2 and 316 Stainless Steel	16
11.	Secondary Fatigue Cracks in Specimen LS-14	17
12.	Changes in Stress Range during Reversed-strain Cycling for Surface Weld Metal	19
13.	Changes in Stress Range during Reversed-strain Cycling for Root Weld Metal	19
14.	Cyclic Stress-Strain Curves from Constant-amplitude, Continuous-cycling Fatigue Tests and Monotonic Tension Test after Cyclic Straining	20
15.	Cyclic Stress-Strain Curves from Constant-amplitude, Continuous-cycling Fatigue Tests for Types 16-8-2 and 316 Stainless Steel	21
A.1.	Scanning-electron Macrograph of Fracture Surface of Specimen LR-3	23
A.2.	Scanning-electron Macrograph of Fracture Surface of Specimen LR-7	23

LIST OF FIGURES

No.	Title	Page
A.3.	Scanning-electron Macrograph of Fracture Surface of Specimen LS-10	24
A.4.	Photomicrographs of a Secondary Crack in Specimen LR-3	24
A.5.	Fractographs of Specimen LR-3	25
A.6.	Fractographs of Specimens LR-4 and LR-5	25
A.7.	Photomicrographs of Main Crack in Specimen LS-14	26
A.8.	Photomicrographs of a Secondary Crack in Specimen LR-7	27
A.9.	Photomicrographs of a Secondary Crack and Internal Damage in Specimen LS-10	27
A.10.	Fractographs of Specimen LR-7	28
A.11.	Fractograph of Specimen LS-10	28
A.12.	Scanning-electron Macrograph of Surface of Specimen 775-L3	29
A.13.	Fractographs of Specimen 775-L3	30
A.14.	Fractographs of Specimens 775-L1 and -L14	30
A.15.	Photomicrographs of Internal Damage in Specimens 775-L9, -L14, and -L1	31
A.16.	Macrograph of Cross Section of Specimen 775-L4	32
A.17.	Photomicrograph of an Inclusion in Specimen 775-L14	32

LIST OF TABLES

No.	Title	Page
I.	Chemical Composition of Type 16-8-2 Stainless Steel ASA Weld Metal	9
II.	Results of Fatigue Tests on Type 16-8-2 Stainless Steel ASA Weld-metal As-welded Longitudinal Specimens at 593°C and $\dot{\epsilon} = 4 \times 10^{-3}\ s^{-1}$	13
III.	Fatigue Properties of Types 16-8-2 and 316 Stainless Steel at 593°C and $\dot{\epsilon} = 4 \times 10^{-3}\ s^{-1}$	15
IV.	Type 16-8-2 Stainless Steel ASA Weld-metal Monotonic and Cyclic Tensile Data from Fatigue Tests on As-welded Longitudinal Specimens at 593°C and $\dot{\epsilon} = 4 \times 10^{-3}$ and $4 \times 10^{-4}\ s^{-1}$	18
A.1.	Creep-rupture Test Data for ASA Type 16-8-2 Stainless Steel Weld Metal	23

CYCLIC-DEFORMATION RESISTANCE OF WELD-DEPOSITED TYPE 16-8-2 STAINLESS STEEL AT 593°C

by

D. T. Raske

ABSTRACT

This report presents results from an investigation on the creep-fatigue and cyclic-deformation behavior of Type 16-8-2 (16% Cr-8% Ni-2% Mo) stainless steel weld metal. Tests were conducted in air at 593°C and a strain rate of 4×10^{-3} s^{-1}. Comparisons with data for Type 316 stainless steel base metal indicate that the weld metal has significantly longer fatigue lives for 360-, 1.8×10^3-, and 1.8×10^4-s tension hold-time tests. This is attributed to the fine duplex microstructure of the weld metal that inhibits the growth rate of cracks. Additional studies on the cyclic-deformation behavior of the weld metal indicate that this material is strain-history dependent; therefore a unique cyclic stress-strain curve does not exist. Monotonic tension tests after cyclic straining result in a different stress-strain curve than obtained from companion fatigue tests at various completely reversed constant strain ranges. A comparison of the fracture morphology of creep-fatigue and creep-rupture specimens indicates that differences resulting from these tests can be attributed to different failure mechanisms.

I. INTRODUCTION

Type 16-8-2 (16% Cr-8% Ni-2% Mo) stainless steel weld metal was developed in the 1950's for the fabrication of main-steam-piping used in power-generating plants. At that time, this material fulfilled a need for a weld-metal composition that had good elevated-temperature (~650°C) mechanical properties, would not embrittle on aging, and was not susceptible to solidification cracking.[1] More recently, this material is also undergoing tests to determine its suitability as a filler metal for Liquid Metal Fast Breeder Reactor (LMFBR) components fabricated from Type 316 stainless steel. As a result, Type 16-8-2 weld metal is well characterized in terms of its microstructural, creep-rupture, and monotonic tensile properties.[2-8] However, LMFBR components are operated under conditions in which creep and fatigue damage can occur simultaneously. Therefore the creep-fatigue properties, as well as the cyclic stress-strain properties, are of interest to designers.

The present investigation provides input for a test program to determine the suitability of this material as a filler metal for joining Type 316 stainless steel in the fabrication of the Clinch River Breeder Reactor thermal liner. Thus, the principal objective is to determine the creep-fatigue and cyclic stress-strain properties of Type 16-8-2 stainless steel weld metal deposited by the automatic submerged-arc (ASA) process, and compare the results with existing data on wrought Type 316 stainless steel tested at 593°C. Another goal is to continue development of the equipment and techniques necessary to perform creep-fatigue tests on weld metals.

II. SCOPE

This report contains the results of continuous-cycling and tension hold-time (360, 1.8×10^3, and 1.8×10^4 s) fatigue tests on as-welded Type 16-8-2 stainless steel specimens that were machined longitudinally from the surface and root areas of the weld. All tests were conducted in air at 593°C and at a strain rate $\dot{\epsilon} = 4 \times 10^{-3}\ s^{-1}$. The initial monotonic tensile data and the cyclic stress-strain curves determined from continuous-cycling and incremental-step tests are also included.

III. EXPERIMENTAL PROGRAM

A. Type 316 Stainless Steel Baseline Data

Because variations between different heats and heat treatments can affect the continuous-cycling and creep-fatigue behavior of austenitic stainless steels,[9-11] the comparison base-metal data were confined to those from one heat and heat treatment. The data used as the basis to compare the fatigue behavior of the weld metal were from Heat 65808 of Type 316 stainless steel in the solution-annealed condition[12,13] and are shown in Fig. 1.

B. Materials and Specimens

Using the ASA process, Babcock and Wilcox welded together 25.4-mm-thick Type 316 stainless steel base-metal plates. The weld joint was a single V-groove with a 19-mm root opening and a 20° included angle. Approximately 20 passes were necessary to complete the weld. Table I lists an analysis of the chemical composition of the Type 16-8-2 stainless steel weld metal. The microstructure consists of columnar austenite subgrains epitaxially grown from the base metal as shown in Fig. 2, and separated by ~0.8-3.0% ferrite[6] distributed in the cellular-dendritic pattern illustrated in Fig. 3. Figure 4 shows photomicrographs of the weld metal parallel to each of the three principal directions. These photomicrographs are typical for the material at the center of the weld where the solidification direction is essentially parallel to axis 3. For comparison, Fig. 5 shows the microstructure of the base metal (Heat 65808).

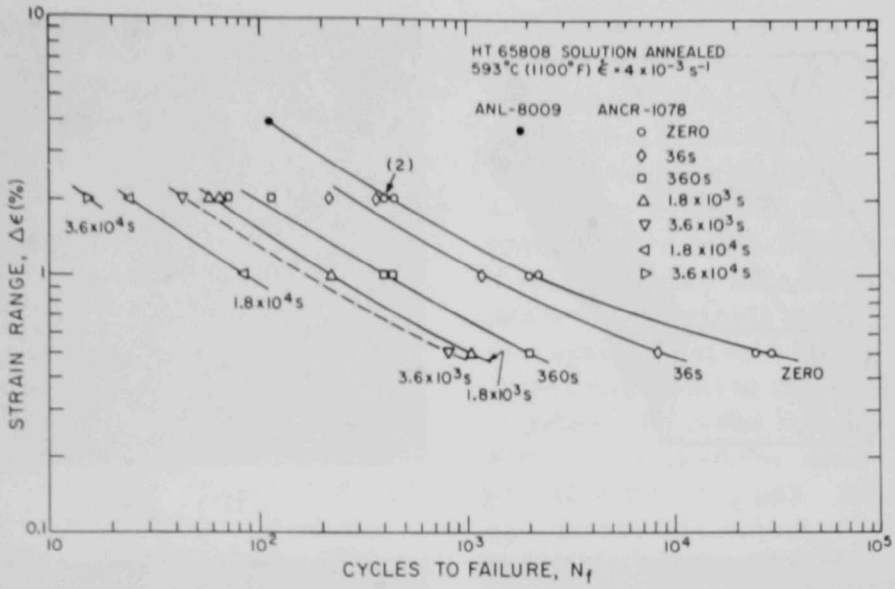

Fig. 1. Total Strain Range vs Cycles to Failure, Showing Effect of Tension Hold Time on Fatigue Life for Type 316 Stainless Steel Baseline Data (Open symbols from Ref. 12, solid symbol from Ref. 13). Neg. No. MSD-63754.

TABLE I. Chemical Composition (weight percent) of Type 16-8-2 Stainless Steel ASA Weld Metal[6]

	C	Mn	P	S	Si	Cu	Ni	Cr	Mo	Ti	Nb	Ta	Co	N	B	V
Weld Center	0.047	1.48	0.026	0.012	0.89	0.09	10.03	14.85	1.76	0.010	0.030	0.03	0.09	0.028	<0.001	0.04
Final Pass	0.047	1.39	0.029	0.014	0.87	0.04	9.27	14.43	1.80	0.013	0.003	0.03	0.09	0.028	<0.001	0.04

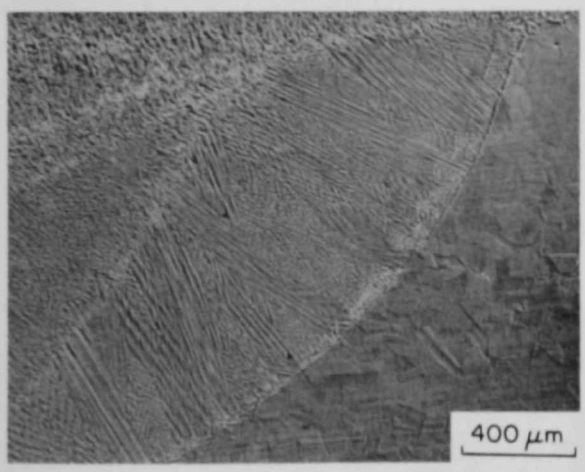

Fig. 2. Macrograph of Fusion Zone between Type 316 Stainless Steel Base Metal and ASA Type 16-8-2 Stainless Steel Weld Metal. Oxalic acid. ANL Neg. No. 306-77-634.

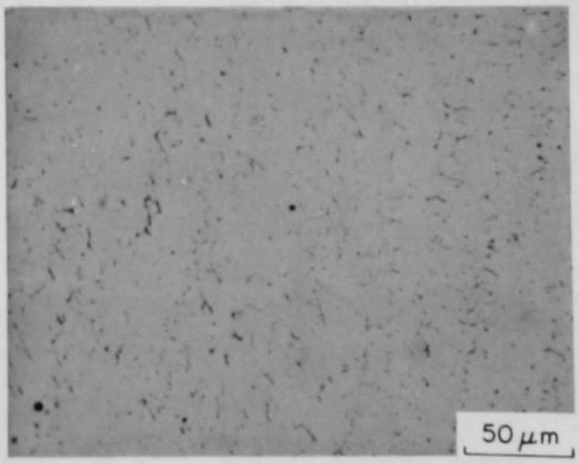

Fig. 3. Distribution of Ferrite in ASA Type 16-8-2 Stainless Steel Weld Metal. 50% HCl. ANL Neg. No. 306-77-638.

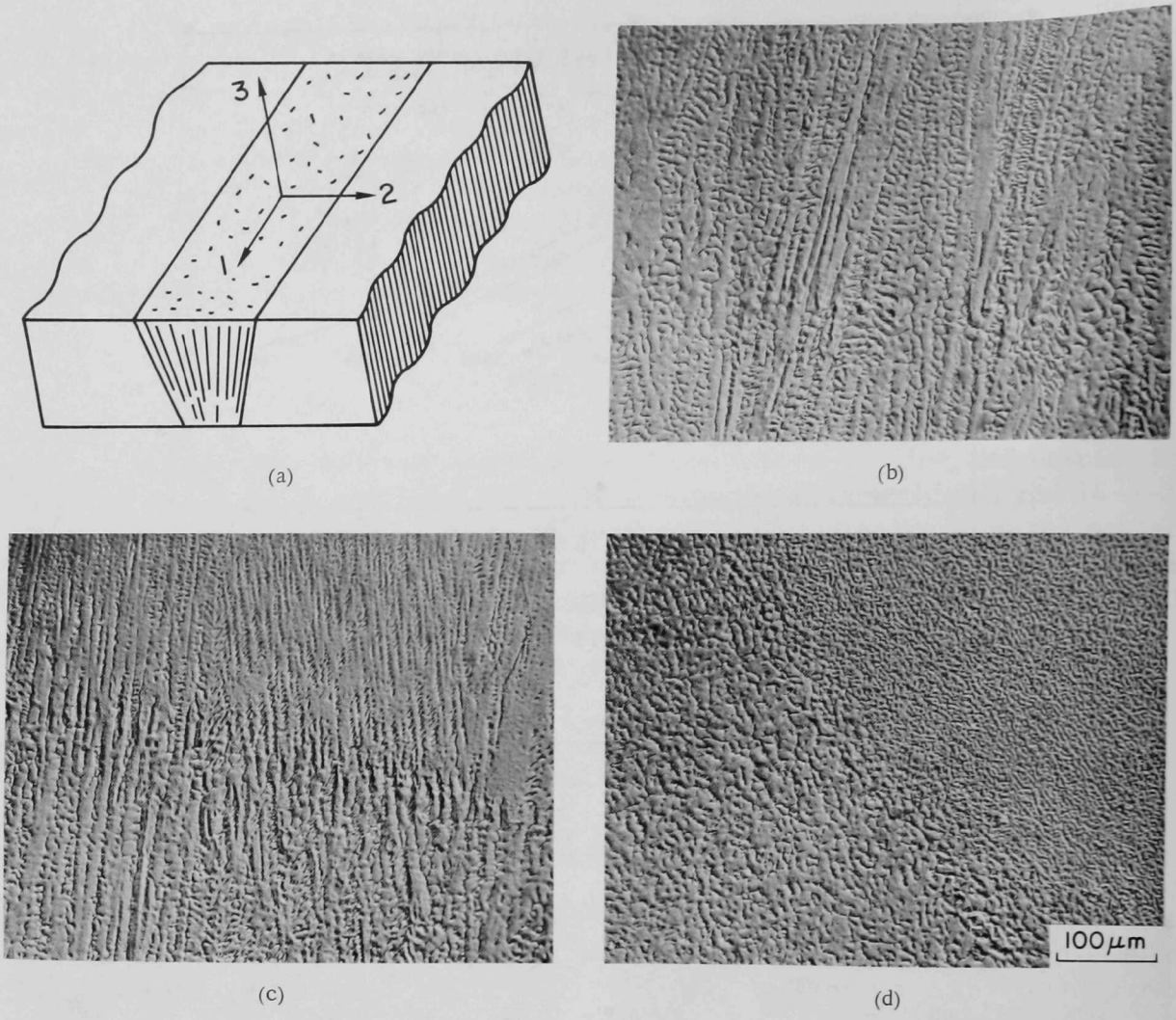

Fig. 4. Microstructure of ASA Type 16-8-2 Stainless Steel Weld Metal. Oxalic acid. (a) Coordinate axes. (b) Parallel to 2-3 plane. (c) Parallel to 3-1 plane. (d) Parallel to 1-2 plane. ANL Neg. No. 306-77-647.

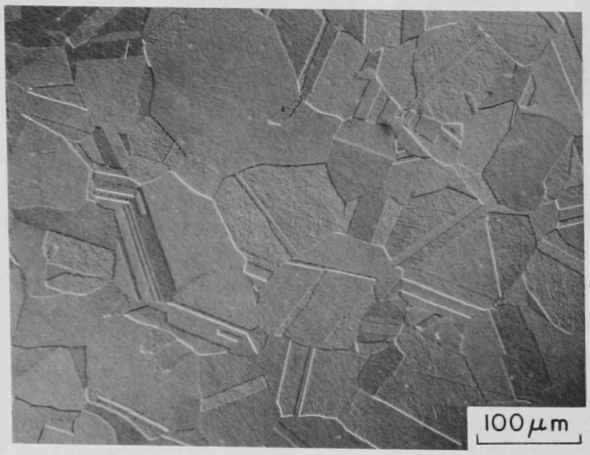

Fig. 5

Microstructure of Type 316 Stainless Steel (Heat 65808 solution annealed). Oxalic acid. ANL Neg. No. 306-77-631.

Axially loaded uniform-gauge specimens were machined from the weld as shown in Fig. 6a. Specimens are designated LS (longitudinal surface) and LR (longitudinal root). The uniform-gauge specimen design was used in lieu of the hourglass specimen traditionally employed in elevated-temperature tests because the weld metal is highly anisotropic and, consequently, a single diametral extensometer and strain computer cannot uniformly control the axial strain. Dimensions of the button-head type specimens used for most of the tests are shown in Fig. 6b. Initially, these specimens were designed without a taper over the 16.76-mm gauge section and were mechanically polished. However, room-temperature tests with strain gauges in the gauge section indicated that the strain at the center of the straight gauge section was ~15% less than the strain controlled by the axial extensometer.

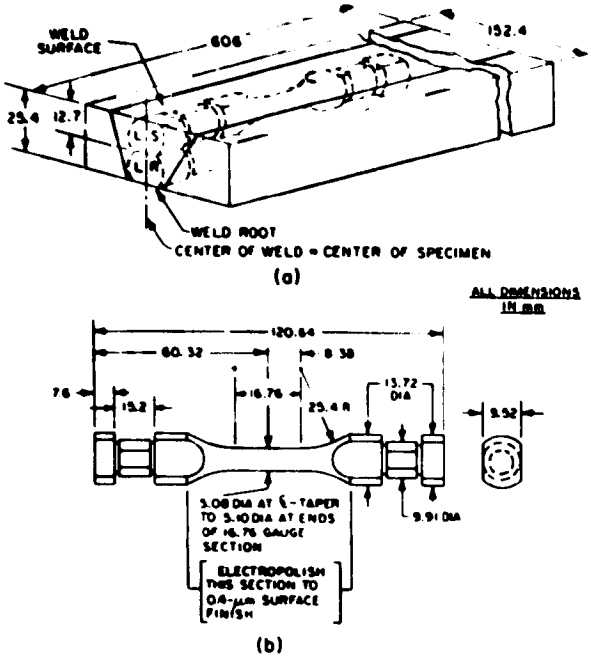

Fig. 6. ASA Type 16–8–2 Stainless Steel Weld-metal Test Specimens. Neg. No. MSD-63753.

Subsequent tests indicated that the taper shown in Fig. 6b would most nearly result in a uniform strain distribution over the gauge section. Mechanical polishing of this material to obtain the surface finish necessary to avoid premature failures proved to be excessively time-consuming. Mechanically polished surfaces with a roughness ≳0.2 μm resulted in failures that appeared to initiate at fine circumferential tool marks. Electropolishing with a solution of 60% phosphoric and 40% sulfuric acid for ~120 s after an initial mechanical polish with 600-grit paper eliminated these problems, although the minimum roughness obtainable was only 0.4 μm

C. Apparatus and Test Procedure

The tests were conducted in an MTS closed-loop hydraulic test machine at 593°C in air with a constant axial strain rate $\dot{\epsilon}$ of 4×10^{-3} s^{-1} using a triangular loading waveform. (These were the same test parameters used for the comparison base-metal tests.) All but one test was started in the compressive direction, usually at a strain rate of 4×10^{-4} s^{-1}. This low strain rate was used because it resulted in an x-y plotter record that simplified calculation of the elastic modulus. The strain rate was increased after the first quarter cycle. This procedure was later abandoned because it was believed to contribute to specimen buckling, which will be discussed later. Failure was defined as complete separation of the specimen.

Most of the specimens were tested in a loading fixture that had a three-post die set to provide accurate alignment during tests.[14] A number of experimental problems were encountered with this gripping arrangement. Unless the entire load train and specimen were in exact alignment, delayed buckling of the specimen occurred. Indeed, large bending strains could be induced in a specimen if the upper clamping plate bolts were tightened improperly. For these tests, two strain gauges 90° apart were used on each specimen in an area outside the gauge section to facilitate mounting with a minimum of bending before testing. This procedure was effective for eliminating the buckling problems experienced in earlier tests. At present, a self-aligning liquid-metal grip, shown in Fig. 7, is used for testing. Using a precision-machined alignment specimen with strain gauges attached, the bending strains caused by this gripping arrangement were ~2% of the total strain range. The button-head specimens used in the previous tests were modified for this grip by threading the ends.

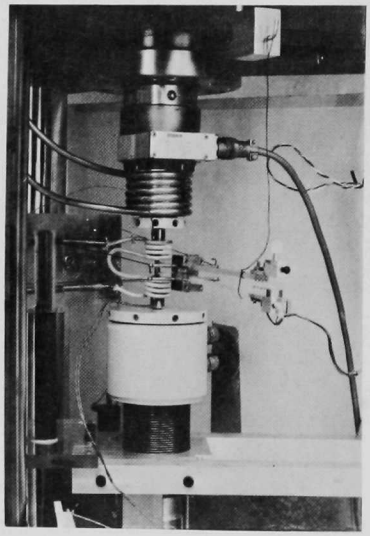

Fig. 7

Liquid-metal Grip Showing a Specimen Surrounded by Induction-heating Coil and with Axial Extensometer Attached. Neg. No. MSD-64053.

Specimen heating was accomplished by an induction coil operated at 455 kHz. The coil, shown in Fig. 7, was constructed to provide a uniform temperature distribution (±4°C) over the gauge section of the specimen. Power to the coil was provided by a Lepel high-frequency induction heater and was controlled by a thermocouple welded to the specimen. One additional thermocouple was placed on each side of the gauge section to monitor the temperature during tests. All thermocouples were located in the transition region 11.4 mm from the center of the gauge section to avoid initiation of cracks at the thermocouple welds.

The temperature profile over the gauge section and the control-thermocouple temperature were determined from 16 equally spaced thermocouples welded to a facsimile Type 316 stainless steel specimen. However, a later temperature profile on a Type 16-8-2 stainless steel specimen indicated that the control thermocouple on samples of this material must be

operated at a higher temperature to obtain the desired 593°C over the gauge section. Consequently, several tests were conducted at a gauge-section temperature of 584°C. This, however, did not appear to affect the results, as will be shown in the next section.

An axial extensometer with a gauge length of 11.68 mm was used to control longitudinal strain in the specimen. This extensometer, shown in Fig. 7, is supported by counterweights, and the extensometer tips are held in place on the specimen by friction. To date, no slippage has been observed nor have there been any failures under the extensometer tips. Moreover, the locations of the crack-initiation sites around the circumference and along the gauge section of the specimens are random, indicating an absence of any systematic specimen misalignment.

IV. RESULTS AND DISCUSSION

A. Continuous-cycling and Tension Hold-time Fatigue Tests

The results of this part of the investigation are listed in Table II. Figure 8 compares these results with the strain-life curves from the Type 316 stainless steel baseline data. As shown in this figure, the cyclic life of the

TABLE II. Results[a] of Fatigue Tests on Type 16-8-2 Stainless Steel ASA Weld-metal As-welded Longitudinal Specimens at 593°C and $\dot{\varepsilon} = 4 \times 10^{-3}\ s^{-1}$

Specimen Number	Location in Weld	Axial Strain Range, %		Tensile Hold Time, s	Stress at $N_f/2$, MPa		Fatigue Life		Remarks
		$\Delta\varepsilon_t$	$\Delta\varepsilon_p$		$\Delta\sigma^b$	$\Delta\sigma_r$	N_f	t_f, ks	
LR-12	Root	2.03	1.43	0.0	302.6/299.7	-	367	3.70	-
LS-7	Surface	1.95	1.32	0.0	306.2/303.3	-	636	6.41	c
LS-13	Surface	1.50	0.95	0.0	262.5/267.6	-	1 407	11.04	d,e
LR-4	Root	1.50	1.00	0.0	255.6/250.7	-	1 567	11.88	-
LS-2	Surface	0.99	0.42	0.0	245.3/243.1	-	1 335	6.78	d,e,f
LS-4	Surface	1.00	0.52	0.0	246.3/255.5	-	2 836	14.22	d,e
LR-5	Root	1.00	0.53	0.0	233.3/238.8		3 634	18.06	e
LS-12	Surface	0.51	0.15	0.0	187.4/191.0	-	27 906	69.78	d,e
LR-3	Root	0.50	0.12	0.0	185.7/170.9	-	31 155	77.58	e
LS-15	Surface	0.51	0.15	0.0	172.3/172.3		67 027[g]	168.84	d,e
LR-13	Root	1.00	0.61	360	198.2/218.3	397.1	1 747	637.32	-
LS-14	Surface	1.00	0.64	360	185.8/219.6	383.8	2 759[h]	1006.38	d,e
LR-7	Root	0.51	0.16	360	176.6/203.3	374.9	5 874	2128.98	-
LS-6	Surface	0.50	0.17	360	166.1/154.9	312.8	9 947	3605.80	-
LS-10	Surface	1.50	0.74	1.8×10^3	368.7/366.5	682.3	329	592.86	-
LR-11	Root	1.00	0.63	1.8×10^3	209.9/288.8[i]	414.0[j]	>972[l]	>1750.25[l]	-
LR-10	Root	2.03	1.54	1.8×10^4	237.7/246.5	421.1	>85[k]	~1536	-
LS-8	Surface	1.02	0.62	1.8×10^4	205.4/200.4	367.6	291[l]	4501.30[l]	-

[a] $\Delta\varepsilon_t$ = total strain range, $\Delta\varepsilon_p$ = plastic strain range, $\Delta\sigma$ = total stress range, $\Delta\sigma_r$ = relaxed stress range, N_f = cycles to failure, and t_f = time to failure.
[b] Peak tensile stress/peak compressive stress.
[c] Test started in tensile direction.
[d] Tested at 584°C.
[e] First quarter cycle at $\dot{\varepsilon} = 4 \times 10^{-4}\ s^{-1}$.
[f] Mechanically polished.
[g] Failed at tool mark in transition region, no visible cracks in gauge section.
[h] Machine shut down before failure, many large cracks in gauge section.
[i] Values for cycle 252.
[j] Specimen removed unbroken; specimen overstrained at cycle 253 as a result of programmer malfunction.
[k] Test stopped before failure as a result of programmer malfunction; several cracks in gauge section.
[l] Specimen removed unbroken; no visible cracks in gauge section.

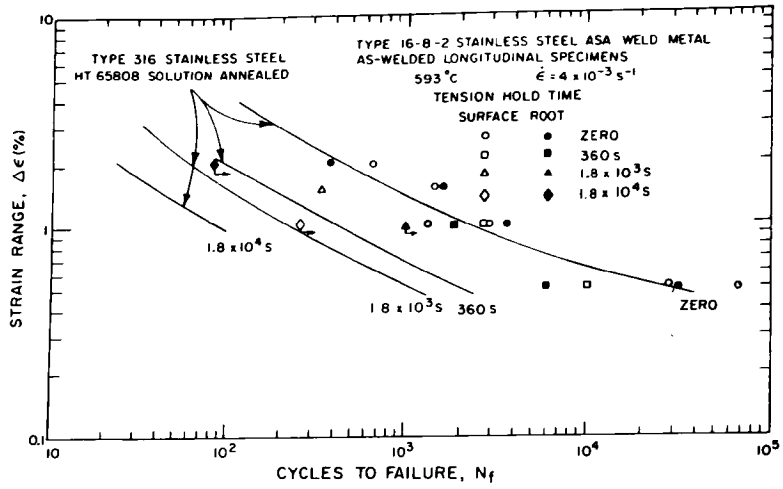

Fig. 8. Total Strain Range vs Cycles to Failure for ASA Type 16–8–2 Stainless Steel Weld Metal Compared with Type 316 Stainless Steel Baseline Data. Neg. No. MSD–64049.

weld metal is greater than that of the base metal for the imposed strains. One significant exception to this observation is a continuous-cycling test at a total strain range of 1% (specimen LS-2). This specimen was mechanically polished, and, although it is difficult to determine, the failure is believed to have started at a fine circumferential tool mark in the gauge section. As indicated in Table II, the fatigue lives for the specimens tested at 584 and 593°C are not significantly different, and in several cases, specimens tested at 584°C had shorter fatigue lives than those tested at 593°C.

The strain-life behavior of the continuous-cycling data* for the weld metal was determined by techniques outlined by Morrow.[15] This results in an expression that relates the strain range $\Delta\epsilon$ to the fatigue life N_f in the form

$$\Delta\epsilon = \frac{2\sigma_f'}{E}(2N_f)^b + 2\epsilon_f'(2N_f)^c, \tag{1}$$

where

σ_f' = fatigue-strength coefficient,

ϵ_f' = fatigue-ductility coefficient,

b = fatigue-strength exponent,

c = fatigue-ductility exponent,

and

E = elastic modulus.

*Specimen LS–2 was excluded from these data.

Values of σ_f', ϵ_f', b, and c were determined by linear-regression analyses on the logarithms of the elastic- and plastic-strain amplitude with the logarithm of twice the fatigue life and are listed in Table III. Figure 9 is a plot of elastic, plastic, and total strain range versus fatigue life for this material. A similar analysis was performed on the Type 316 baseline data, and the values for its fatigue properties are also listed in Table III. Figure 10 compares the strain-life behavior for these two materials, as calculated using Eq. 1. As shown in this figure, the resistance to cyclic straining, i.e., cyclic life of the weld metal relative to that of the base metal, increases as the strain range decreases. The increasing fatigue resistance of the weld metal relative to that of the base metal at long lives is also reflected by the value of the fatigue strength exponent, b, listed in Table III. Thus, the lower value of b for the weld metal indicates an increased resistance to elastic-strain deformations relative to that of the base metal in the long-life regime. If this trend were to continue, the fatigue life of the weld metal would be one order of magnitude greater than that of the base metal at a strain range of ~0.25%. However, extrapolation beyond a data base is not generally recommended, and it would therefore be inappropriate to speculate on the fatigue behavior of these two materials at strain ranges below those shown in Fig. 8.

TABLE III. Fatigue Properties of Types 16-8-2 and 316 Stainless Steel at 593°C and $\dot{\epsilon} = 4 \times 10^{-3}\ s^{-1}$

Material	Fatigue-strength Coefficient (σ_f'), MPa	Fatigue-ductility Coefficient (ϵ_f')	Fatigue-strength Exponent (b)	Fatigue-ductility Exponent (c)
Type 16-8-2	660.7	0.278	-0.115	-0.528
Type 316[a]	1010.2	0.239	-0.137	-0.516

[a]Elastic modulus = 149.75×10^3 MPa

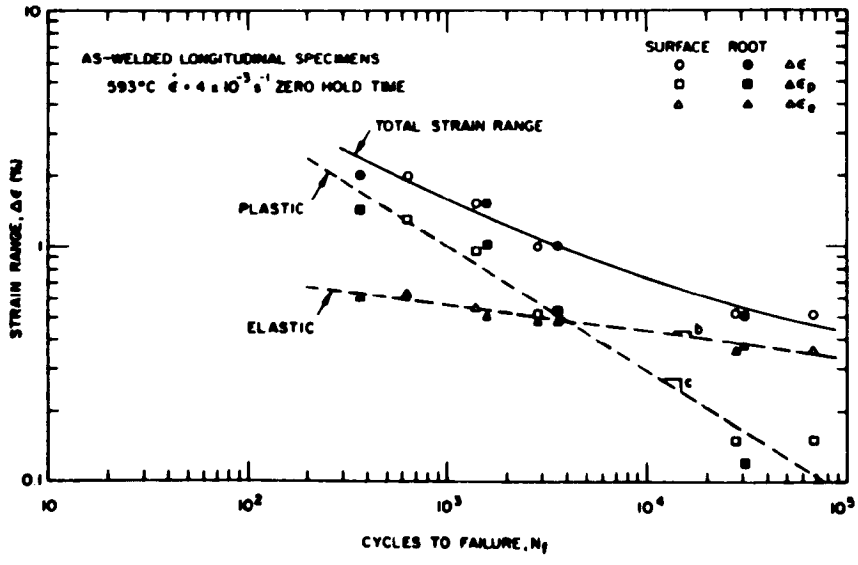

Fig. 9. Ranges of Total, Elastic, and Plastic Strain vs Cycles to Failure for ASA Type 16-8-2 Stainless Steel. Neg. No. MSD-64051.

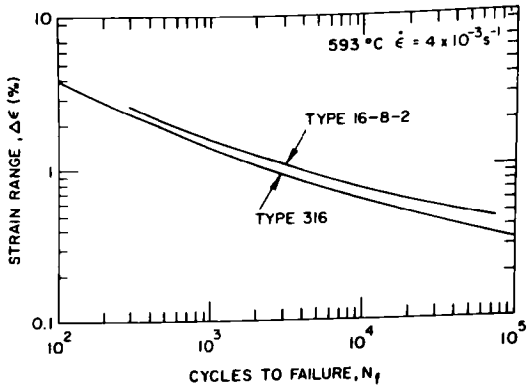

Fig. 10. Total Strain Range vs Cycles to Failure for Types 16-8-2 and 316 Stainless Steel. Neg. No. MSD-64052.

The results of the 360-, 1.8 x 10^3-, and 1.8 x 10^4-s tension hold-time tests are particularly significant because the fatigue life for the weld metal is three to seven times longer than that for the base metal when tested under the same conditions. This was unexpected since the creep-rupture properties of the weld metal are significantly poorer than the average properties for Type 316 stainless steel at 566 and 650°C.[6] Moreover, it has been statistically established that heats of a similar austenitic stainless steel base metal, Type 304, with poor creep properties also tend to exhibit poorer than average creep-fatigue properties.[10] Thus, the correlation between creep and creep-fatigue behavior observed in base-metal samples is apparently not valid for weld metals.

One mechanism that may explain the difference between the weld metal and base metal is the mode of fatigue-crack propagation in these materials. The results of crack-growth-rate studies on stainless steel weld- and base-metal samples indicate that the weld metal has significantly lower crack-growth rates than the base metal, particularly at 593°C.[16-18] This difference is attributed to the fine duplex delta ferrite-austenite microstructure in the weld metal, which, with its many phase boundaries, inhibits the growth rate of cracks.

Evidence that the fine microstructure of the weld metal is responsible for the observed differences in the fatigue lives of this material and the base metal was obtained from a posttest examination of the weld-metal specimens. One specimen (LS-14), which did not separate at failure, was sectioned normal to the main crack and metallographically examined over the entire gauge section. All 88 cracks observed along both sides of the gauge section appeared to initiate at phase boundaries that intersected the surface of the specimen. Of this total, more than one-third of the cracks stopped at either a phase-boundary triple point or a sharp break in an individual phase boundary, as shown in Fig. 11. The propagation for the largest and several secondary cracks appeared to be almost entirely within the austenite matrix after a length of ~0.03 mm was attained within a phase boundary.

Although there was some evidence of interphase cracking, a major amount of crack growth in the weld metal specimens apparently occurred by a mechanism similar to transgranular cracking in wrought materials. (See the appendix for a discussion of the fracture morphology of creep-fatigue and creep-rupture specimens.) In contrast, the mode of crack propagation for the Type 316 stainless steel tested under the same conditions of tension hold time was reported to be intergranular.[12]

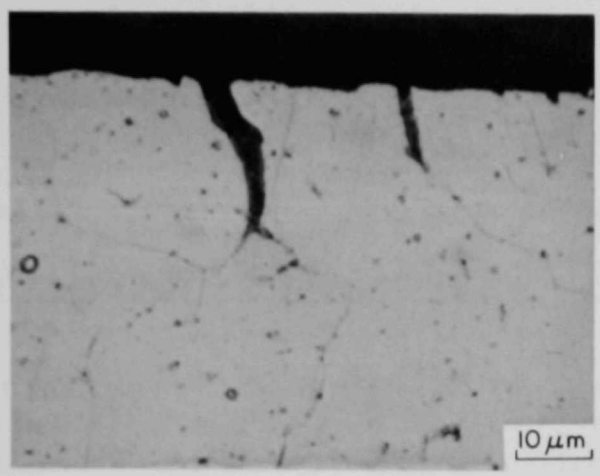

Fig. 11

Secondary Fatigue Cracks in Specimen LS-14. 50% HCl. ANL Neg. No. 306-77-633.

Another mechanism that could account for the differences in cyclic lives between the weld metal and the base metal has been attributed to microstructural differences that affect the number of cycles required to initiate a macroscopic crack.[19] In a study on the low-cycle fatigue behavior of cast and wrought austenitic alloys, fatigue-striation counts indicated that both materials spent approximately the same fraction of life initiating a macroscopic crack; however, the total life of the cast material was three to twenty times as great as the wrought material. This suggests that the cast material has a much greater resistance to crack initiation than the wrought material. A similar study using the results of the present investigation was not possible because the weld-metal specimens did not have striated areas that were continuous over the cross section (see the appendix), and these data were unavailable for the base-metal specimens.

Differences in fatigue lives attributed to nonmechanistic factors must also be considered. For example, they might be attributed to the fact that the weld-metal specimens were electropolished before testing, whereas the base-metal specimens used for comparison were mechanically polished. However, the base-metal specimens were polished longitudinally to a 0.2-μm finish[20] and, as stated previously, the electropolished finish was only 0.4 μm. In addition, for the same degree of surface roughness, the difference between the low-cycle fatigue life for mechanical and electropolished specimens is insignificant.[21]

Another potential source for the dissimilarity between these data may be the method of beginning the tests. All but one of the Type 316 stainless steel tests were begun with the first quarter-cycle in tension. In contrast, all but one of the weld-metal tests were begun in the compressive direction. Although it had been reported that tests begun in tension would result in somewhat lower fatigue lives,[14] recent studies[10] indicate that no statistically significant difference exists between tests begun in either manner. (Unpublished research by myself also supports this conclusion.)

Finally, size effects also can be eliminated as a contributing factor to the observed differences in fatigue lives of the base and weld metal. A size effect based on the volume of the test specimen has been shown to exist, but the volume differences must be larger than those in the present study.[22] Moreover, the specimens with the largest volume (the uniform-gauge weld-metal specimens) would have the shortest fatigue lives, which was not observed.

B. Initial Monotonic Tensile Data and Cycle-dependent Changes in Mechanical Properties

Table IV lists the monotonic 0.2% offset yield strengths and the elastic modulus for the ASA Type 16-8-2 stainless steel weld metal as determined from the initial portion of the first-cycle hysteresis loops. These results indicate that the metal from the root of the weld has a higher yield strength than that from the weld surface. This is consistent with results obtained at Oak Ridge National Laboratory for this material at 565 and 650°C.[6] A prominent feature in the present data is the large scatter associated with the yield strength of the surface weld metal (more than twice that of the root weld metal). The scatter is probably due to differences in composition, structure, and local properties that result from the variety of thermal histories that occur in various locations of multipass weldments.[2,4] As expected, the elastic modulus exhibits relatively little scatter for these tests and is not statistically different for the surface and root weld metal.

TABLE IV. Type 16-8-2 Stainless Steel ASA Weld-metal Monotonic and Cyclic Tensile Data from Fatigue Tests on As-welded Longitudinal Specimens at 593°C and $\dot{\epsilon} = 4 \times 10^{-3}$ and 4×10^{-4} s^{-1}

Location in Weld	Monotonic 0.2% Offset Yield Strength (σ_{ys}), MPa	Elastic Modulus (E) x 10^3, MPa	Cyclic Properties[a]		
			0.2% Offset Yield Strength (σ'_{ys}), MPa	Strength Coefficient (K'), MPa	Strain-hardening Exponent, n'
Surface	214.1[b]	99.10[c]	231.9/270.3	688.0/475.3	0.175/0.094
Root	237.2[d]				

[a]Upper value from companion tests at constant strain ranges, lower value from monotonic tension tests after spectrum straining.
[b]Standard deviation = 40.90 MPa (6 tests).
[c]Standard deviation = 5.75 MPa (21 tests).
[d]Standard deviation = 18.88 MPa (7 tests).

Figures 12 and 13 show the cyclic hardening and subsequent softening of the weld metal as a function of strain range and cycles. Note the widely differing values for the surface-weld-metal stress range in Fig. 12. This is consistent with the large scatter in the monotonic yield-strength values discussed earlier. Beyond the last data point shown in these figures, the tensile-stress amplitude drops to zero as failure of the specimen occurs.

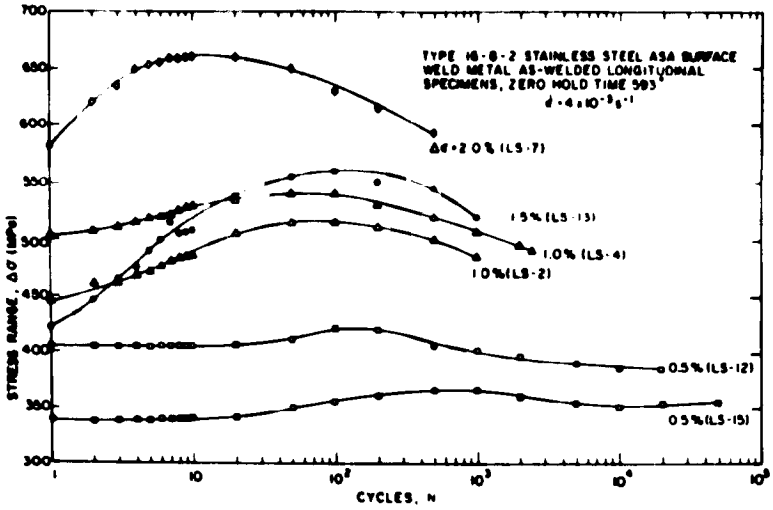

Fig. 12. Changes in Stress Range during Reversed-strain Cycling for Surface Weld Metal (Specimen numbers in parentheses). Neg. No. MSD-63951.

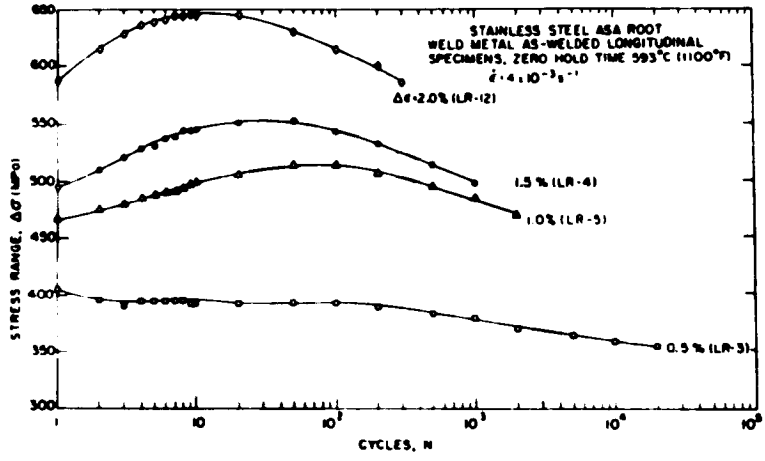

Fig. 13. Changes in Stress Range during Reversed-strain Cycling for Root Weld Metal (Specimen numbers in parentheses). Neg. No. MSD-63950.

The cyclic stress-strain curves shown in Fig. 14 were determined by two methods.[23] The lower curve (solid line) was obtained from the constant-amplitude, continuous-cycling fatigue-test data. A linear regression analysis was performed on the logarithms of the half-life stress $\Delta\sigma/2$ and plastic-strain amplitudes from fatigue tests on both the surface and root weld metal. The results were of the form

$$\Delta\sigma/2 = K'(\Delta\epsilon_p/2)^{n'}, \qquad (2)$$

where

K' = cyclic strength coefficient,

$\Delta\epsilon_p$ = plastic-strain range,

and

n' = cyclic strain-hardening exponent.

Values of K', n', and the cyclic 0.2% offset yield strength are listed in Table IV. The cyclic stress-strain curve was then calculated for the strain amplitude $\Delta\epsilon/2$ using the relation[24]

$$\Delta\epsilon/2 = \Delta\epsilon_e/2 + \Delta\epsilon_p/2 = \Delta\sigma/2E + (\Delta\sigma/2K')^{1/n'}, \tag{3}$$

where

$\Delta\epsilon_e$ = elastic-strain range

and

E = elastic modulus.

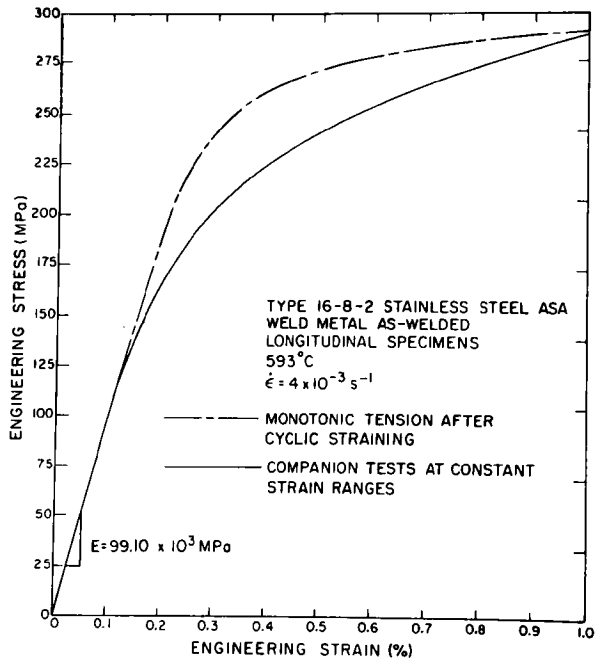

Fig. 14

Cyclic Stress-Strain Curves from Constant-amplitude, Continuous-cycling Fatigue Tests and Monotonic Tension Test after Cyclic Straining. Neg. No. MSD-63952.

Initially, this exercise was performed for the surface and root weld metal individually. However, little difference exists between the calculated curves, particularly at low strains (<0.5%); thus, the data were combined to produce a single curve. At strains >0.5% (strain ranges >1.0%), the surface weld metal has slightly higher cyclic strength values, but the difference is not sufficiently large, nor do adequate data exist to justify separate cyclic stress-strain curves.

The upper curve (broken line) in Fig. 14 was obtained from a monotonic tension test after cyclic straining on a single root-weld-metal specimen. The preliminary straining consisted of blocks of gradually increasing and then decreasing strain amplitudes, i.e., incremental step tests interspersed with blocks of constant strain-range cycling. A total of ~2100 cycles at strain ranges between 0.2 and 2.0% and a constant axial strain rate of $4 \times 10^{-3}\ s^{-1}$ were imposed on the specimen before the monotonic tension test. Values of K' and n' for this stress-strain curve were determined by back-fitting incremental values of the logarithms of stress and plastic strain from the curve in Fig. 14 to the form of Eq. 2 by a linear regression analysis. These values, as well as 0.2% offset yield strength, are also listed in Table IV.

Normally the cyclic stress-strain curve for a given material can be generated by several methods, including those described above, which usually produce approximately the same results.[23] However, some materials, notably Type 304 stainless steel, respond differently to various loading histories; thus, a unique cyclic-strain curve does not exist.[9,25] Since the material used in the present investigation is also an austenitic stainless steel, the different cyclic stress-strain curves shown in Fig. 14 were not unexpected. Although these curves provide widely different values of inelastic strain for a given stress, they both can be of value to designers. For example, if the anticipated loadings on a structural component were such that both large and small strain excursions would occur randomly, then the upper curve of Fig. 14 would be appropriate for characterization of these materials. If, however, the loadings were cyclically constant or increasing, the lower curve would be suitable for design purposes.

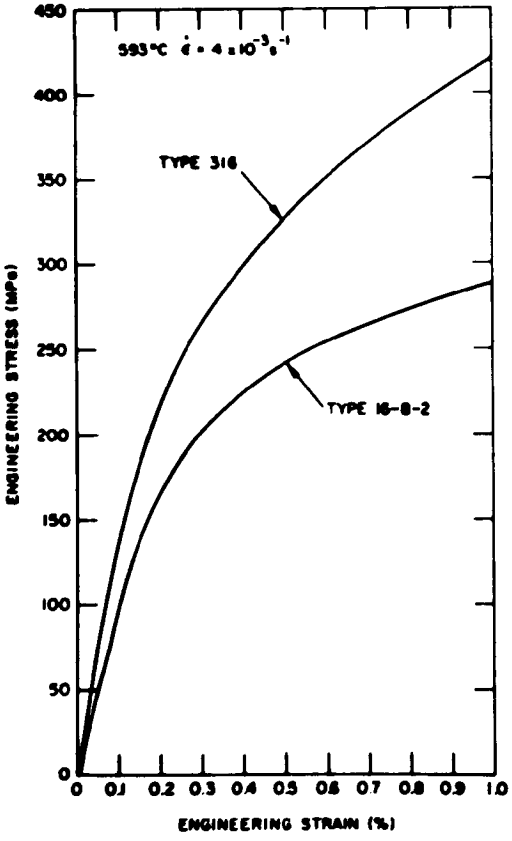

Fig. 15

Cyclic Stress-Strain Curves from Constant-amplitude, Continuous-cycling Fatigue Tests for Types 16-8-2 and 316 Stainless Steel. Neg. No. MSD-64050.

Figure 15 compares the cyclic stress-strain curves for Type 16-8-2 longitudinal weld metal with the Type 316 stainless steel baseline data. Both curves in this figure were obtained from constant-amplitude, continuous-cycling fatigue-test data for each material. Although cyclic stress-strain data for this weld-metal transverse to the welding direction are unavailable, results from monotonic tension tests at 566 and 650°C indicate the 0.2% offset yield strengths are approximately equal to values for specimens longitudinal to the welding direction.[6] Moreover, studies on the mechanical properties of Type 308 stainless steel weld metal indicate that the

elastic-modulus transverse to the welding direction is more nearly equal to that of the base metal (~140-150 x 10^3 MPa).[26]

Therefore, the cyclic stress-strain curve for Type 16-8-2 weld-metal transverse to the welding direction would probably be similar to that of the base metal at low strains (~0.1%) and significantly lower, as is that of the longitudinal weld metal, at higher strains. This may be troublesome for designers, particularly for components that contain circumferential welds operating where fluctuating loads are present. For example, a pipe with circumferential welds and end constraints undergoing thermal cycling would also be subject to cyclic loads. In such situations, the cyclic strains would tend to be concentrated in the weld metal. Thus, the weld would behave in a manner analogous to that of a mild geometric stress concentration. However, this can be offset by the much better creep-fatigue resistance of the weld metal raltive to the base metal.

V. CONCLUSIONS

Cyclic strain-control tests using constant amplitude and tensile hold-time loading waveforms lead to the following conclusions regarding the fatigue resistance and cyclic-deformation behavior of ASA Type 16-8-2 weld metal at 593°C.

a. The resistance of this material to axial strain-controlled, constant-amplitude, continuous-cycling fatigue-test loadings is greater than that of Type 316 stainless steel base metal (Heat 65808) in the solution-annealed condition. Moreover, a comparison of the strain-life curves for these materials indicates that the resistance to cyclic straining of the weld metal relative to that of the base metal increases as the strain range decreases.

b. For 360-, 1.8 x 10^3-, and 1.8 x 10^4-s tension hold-time fatigue tests, the cyclic life of this material is three to seven times as long as that of Type 316 stainless steel. This is attributed to the fine duplex microstructure of the weld metal that inhibits the growth rate of cracks.

c. The correlation between resistance to static creep rupture and resistance to creep-fatigue failures previously observed in Types 304 and 316 stainless steel base metals is not observed for this weld metal.

d. This material is strain-history-dependent; therefore, a unique cyclic stress-strain curve does not exist. Monotonic tension tests after cyclic straining result in a different stress-strain curve than obtained from companion fatigue tests at various completely reversed constant strain ranges.

APPENDIX

Metallographic and Fractographic Analysis of Creep-fatigue and Creep-rupture Specimens

As indicated in Sec. IV, the results of the creep-fatigue tests conducted in this investigation are not consistent with creep-test results obtained at Oak Ridge National Laboratory (ORNL).[6] Because of this, representative samples from this investigation and several creep samples from ORNL[27] were examined to determine whether the differences in test results could be attributed to differences in the fracture morphology. The creep-rupture specimens listed in Table A.1 were used for part of this study.

TABLE A.1. Creep-rupture Test Data for ASA Type 16-8-2 Stainless Steel Weld Metal[27]

Specimen Number	Location in Weld	Temperature, °C	Stress, MPa	Rupture Time, ks	Elongation, %
775-L1	Surface	650	138	1722.6	42.5
775-L14	Root	650	138	2193.8	44.2
775-L9	Root	566	276	753.5	23.3
775-L3	Surface	566	241	2519.3	26.2

Figures A.1-A.3 are scanning-electron macrographs of typical fracture surfaces from continuous cycling and tension hold-time fatigue tests. The fracture surfaces of the specimens subjected to continuous cyclic loadings (Fig. A.1) show little of the columnar substructure of the weld; the specimens subjected to hold times (Figs. A.2 and A.3) show surfaces that are more nearly

Fig. A.1. Scanning-electron Macrograph of Fracture Surface of Specimen LR-3 ($\Delta\varepsilon$ = 0.5%, t_H = 0, solidification direction approximately vertical). ANL Neg. No. 306-77-635.

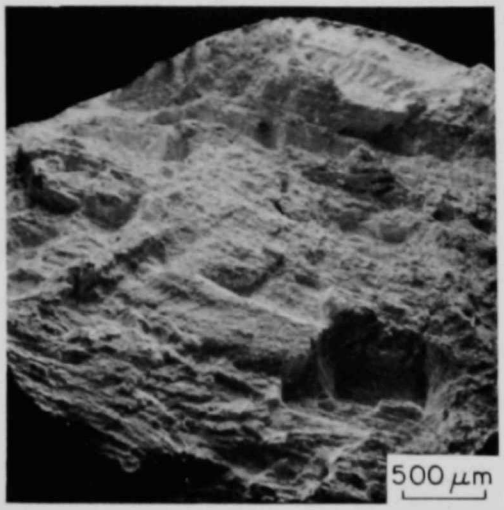

Fig. A.2. Scanning-electron Macrograph of Fracture Surface of Specimen LR-7 ($\Delta\varepsilon$ = 0.5%, t_H = 360 s, solidification direction approximately horizontal). ANL Neg. No. 306-77-632.

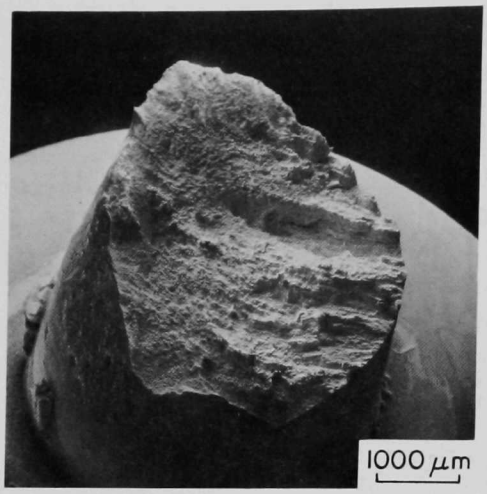

Fig. A.3

Scanning-electron Macrograph of Fracture Surface of Specimen LS-10 ($\Delta\varepsilon$ = 1.5%, t_H = 1.8 x 10^3 s, solidification direction approximately horizontal). ANL Neg. No. 306-77-636.

related to the local substructure. These observations are also supported by the results of metallographic examinations on specimens that were sectioned parallel to the loading axis, and scanning-electron fractographs of the fracture surfaces.

For continuous cyclic loadings, few secondary cracks were observed on the sides of the specimens, and when present, they appeared to propagate within the austenite matrix with no observable internal cracking, or damage, ahead of the crack tip. This is illustrated in Fig. A.4, which shows a 0.5-mm-long secondary crack in specimen LR-3 ($\Delta\varepsilon$ = 0.5%, tensile hold time t_H = 0). Fractographs of the surface of this specimen near the crack origin are shown in Fig. A.5. The fine fatigue striations and dimpled appearance shown in this

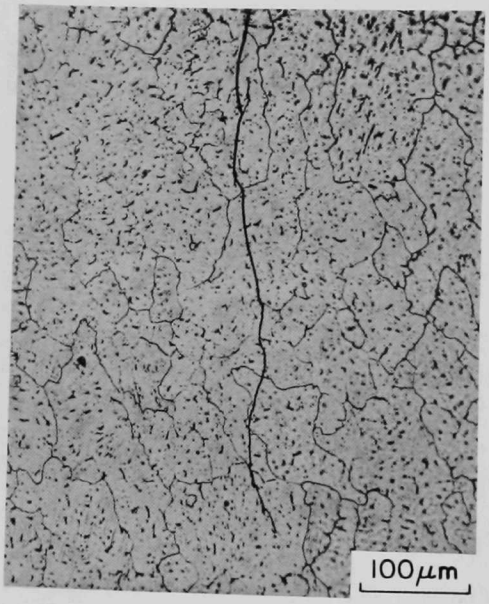

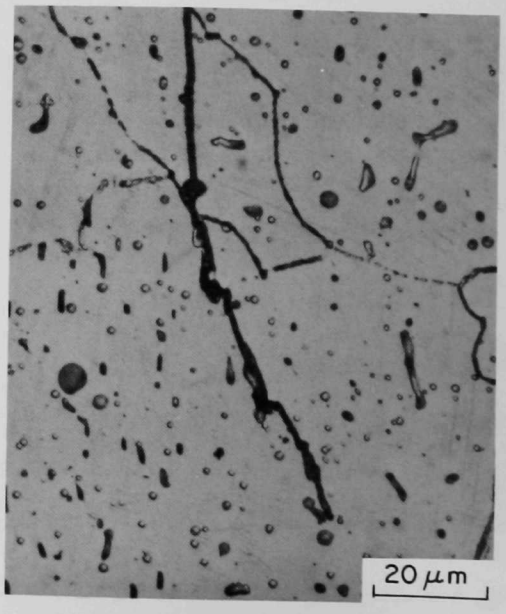

Fig. A.4. Photomicrographs of a Secondary Crack in Specimen LR-3 ($\Delta\varepsilon$ = 0.5%, t_H = 0). Oxalic acid. ANL Neg. No. 306-77-644.

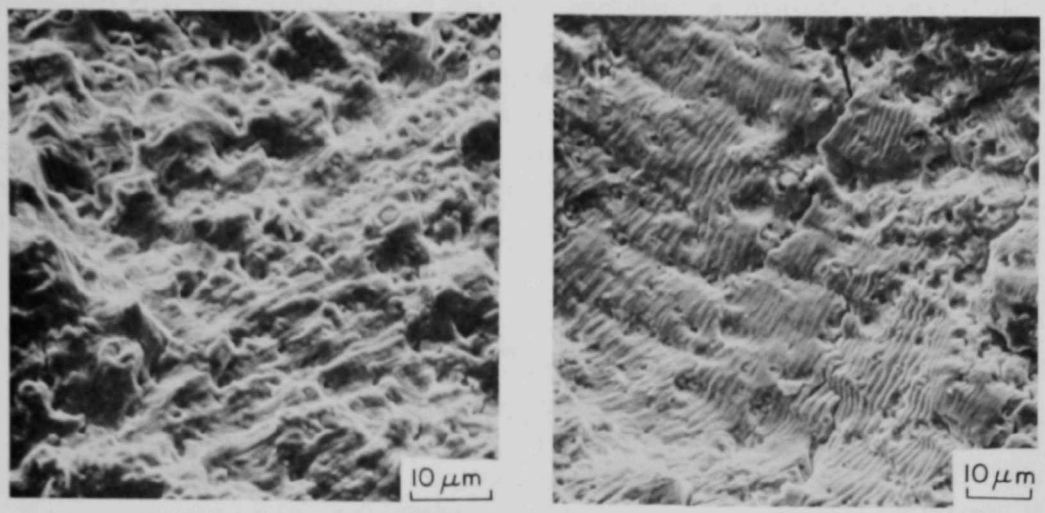

Fig. A.5. Fractographs of Specimen LR-3 ($\Delta\varepsilon$ = 0.5%, t_H = 0). ANL Neg. No. 306-77-648.

figure are typical of the features observed near the crack origin on the other continuous-cycling specimens tested at a low strain range. Away from the crack origin, the fracture surface is generally featureless with some areas showing the dimpled appearance characteristic of ductile failures. These fracture features, which have also been observed in a ferritic weld metal, have been attributed to a change from slow to rapid cyclic crack propagation.[28] Similar features are also visible on specimens tested at higher strain ranges ($\Delta\varepsilon \geq 1\%$), except that the striated areas are more numerous and the spacing between striations increases with the distance from the crack origin, as shown in Fig. A.6. However, there are very few areas like those shown in Fig. A.6 where the striations are well defined.

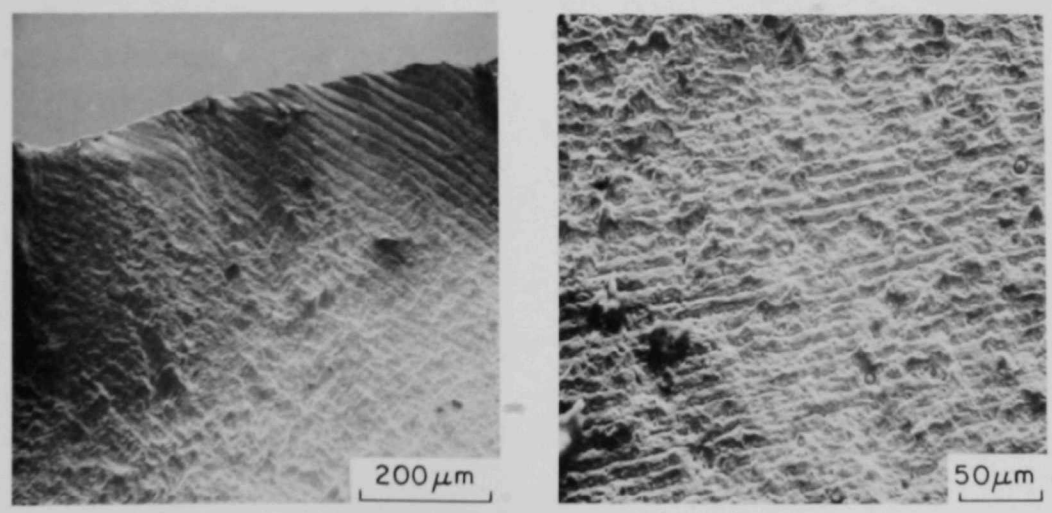

(a) Near final rupture area

(b) Near crack origin

Fig. A.6. Fractographs of Specimens (a) LR-4 ($\Delta\varepsilon$ = 1.5%, t_H = 0), and (b) LR-5 ($\Delta\varepsilon$ = 1.0%, t_H = 0). ANL Neg. No. 306-77-643.

In tests containing a hold time at the peak tensile strain, the number of surface cracks and amount of internal damage at the phase boundaries increased as the hold time increased. Figure A.7 shows the main crack and interphase cracking beyond the crack tip in specimen LS-14 ($\Delta\epsilon$ = 1%, t_H = 360 s). The internal damage is even more pronounced in specimens with the same hold time, but with a longer test duration, as shown in Fig. A.8 for specimen LR-7 ($\Delta\epsilon$ = 0.5%, t_H = 360 s). At longer hold times, the number of surface cracks greatly increased, as did the internal damage.

Specimen LS-10 ($\Delta\epsilon$ = 1.5%, t_H = 1.8 x 10^3 s), shown in Fig. A.9, had numerous long internal phase-boundary cracks and surface cracks, which partly followed the interphase boundaries. The surfaces of this specimen were also "rumpled" parallel to the specimen axis, much like the surfaces of the creep-rupture specimens obtained from ORNL. The fracture surfaces of the 360-s tensile-hold-time specimens varied greatly in observable details, although every specimen examined had some features that appeared related to the substructure of the weld.

Only one specimen, LR-7, shown in Fig. A.10, exhibited a large number of fatigue striations on its surface. Others had more areas that had features of ductile tearing and shear as well as areas of interphase fracture. Specimen LS-10 had a fracture surface consisting of areas that had striations and areas that appeared to be interphase boundaries. A typical region exhibiting these features is shown in Fig. A.11. In all cases, these areas were separated by secondary cracks. Results of an energy-dispersive X-ray analysis of these

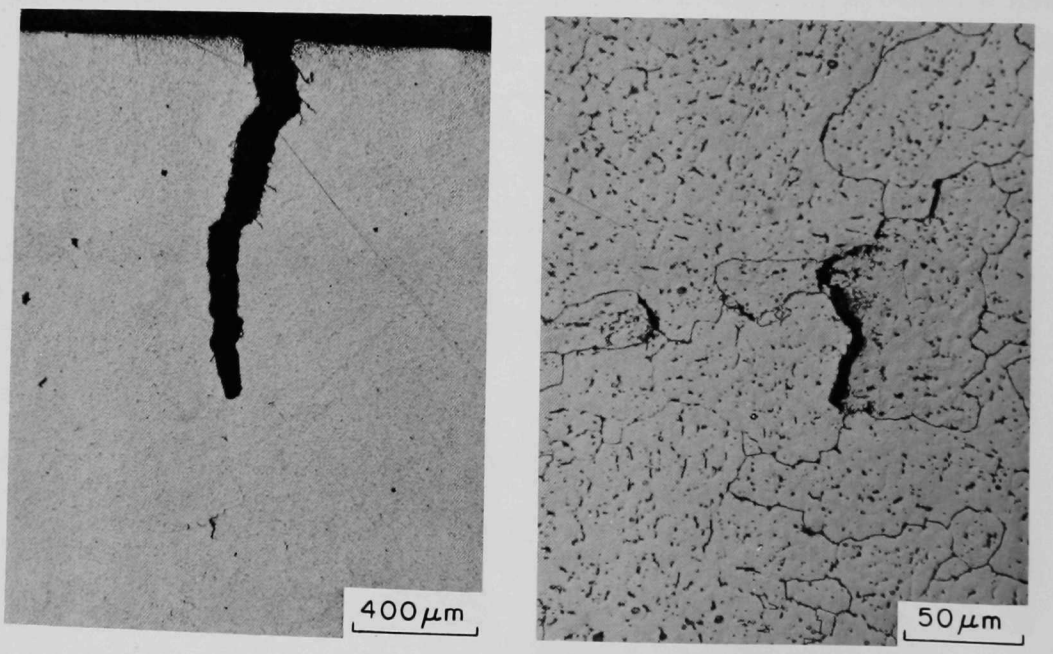

(a) Main crack

(b) Damage beyond main-crack tip

Fig. A.7. Photomicrographs of Main Crack in Specimen LS-14 ($\Delta\epsilon$ = 1.0%, t_H = 360 s). Oxalic acid. ANL Neg. No. 306-77-626.

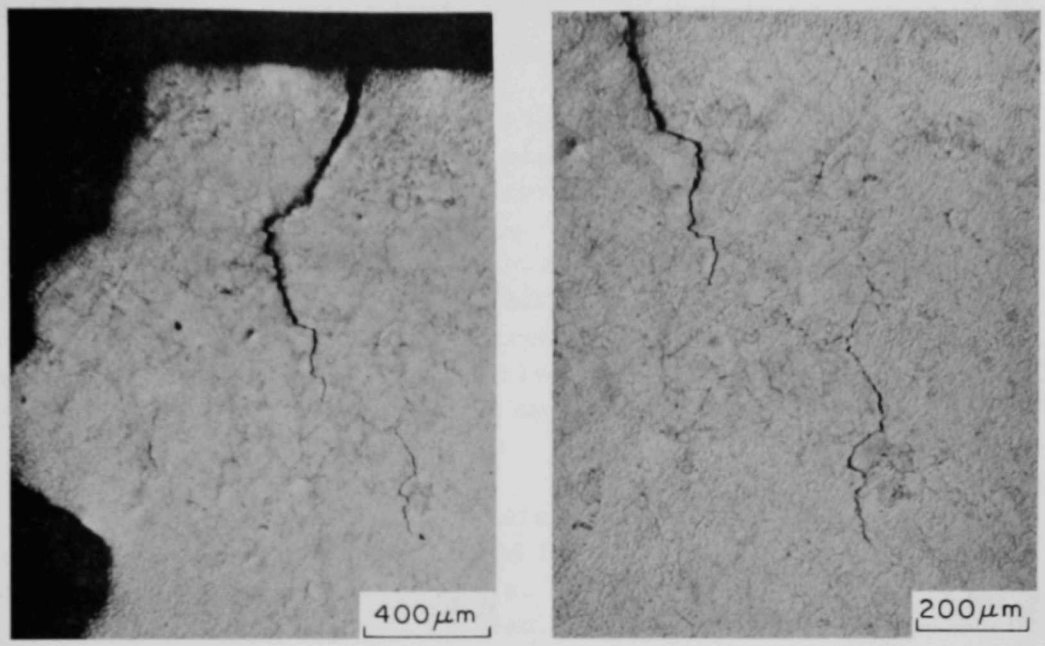

Fig. A.8. Photomicrographs of a Secondary Crack in Specimen LR-7 ($\Delta\varepsilon$ = 0.5%, t_H = 360 s). Oxalic acid. ANL Neg. No. 306-77-627.

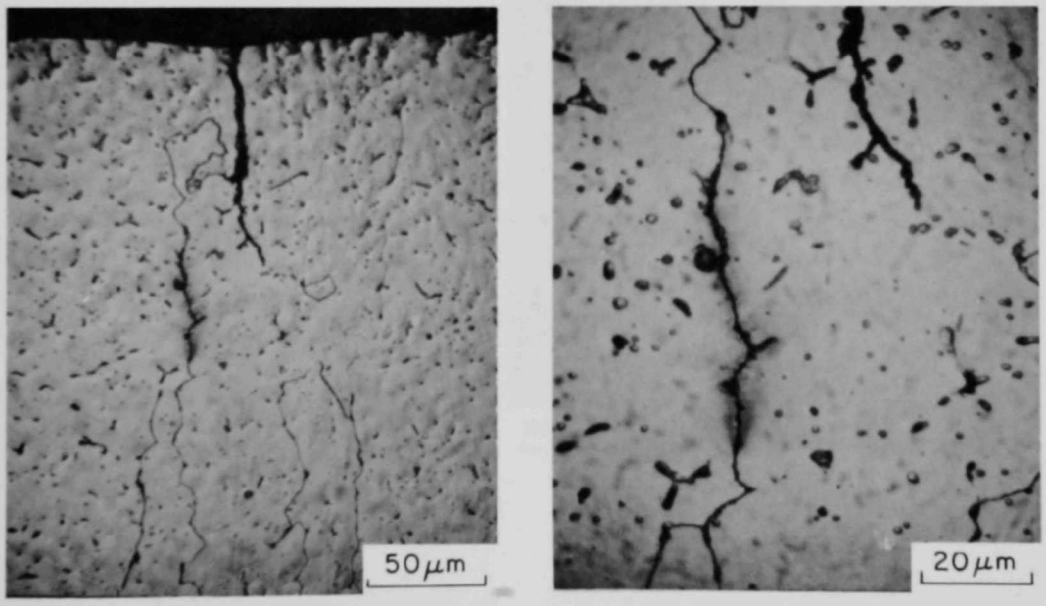

Fig. A.9. Photomicrographs of a Secondary Crack and Internal Damage in Specimen LS-10 ($\Delta\varepsilon$ = 1.5%, t_H = 1.8 x 10^3 s). Oxalic acid. ANL Neg. No. 306-77-628.

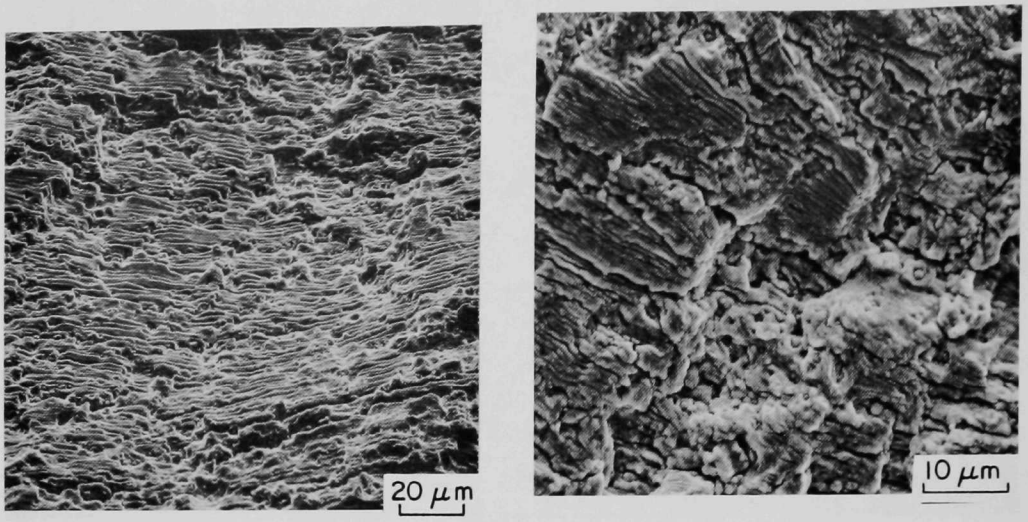

Fig. A.10. Fractographs of Specimen LR-7 ($\Delta\varepsilon$ = 0.5%, t_H = 360 s). ANL Neg. No. 306-77-646.

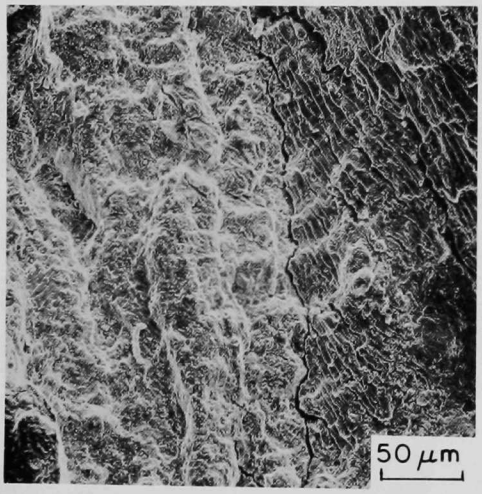

Fig. A.11

Fractograph of Specimen LS-10 ($\Delta\varepsilon$ = 1.5%, t_H = 1.8 x 10^3 s). ANL Neg. No. 306-77-640.

areas indicated that the area containing the striations had a lower chromium and higher nickel content than the area identified as an interphase boundary. It is therefore apparent that the fracture mode of this specimen was by a combination of interphase and matrix cracking.

In contrast with the results for the creep-fatigue tests, the primary fracture mode of the creep-rupture specimens appeared to be entirely due to interphase separation. A typical fracture surface for these specimens is shown in Fig. A.12. Characteristically, these fracture surfaces exhibit features that suggest the failures began internally by tearing along interphase boundaries and, after a sufficient reduction in cross-sectional area, by microvoid coalescence and ductile fast fracture. The former is illustrated in Fig. A.13 by a series of scanning-electron fractographs with increasing magnification. The final rupture of these specimens, shown in Fig. A.14, exhibited both equiaxed and shear-type dimples.

Additional evidence that the failures of these specimens began internally at phase boundaries was obtained from metallographic examination of surfaces parallel to the specimen axis. In all cases, relatively few secondary surface cracks were observed. Instead, all the specimens listed in Table IV exhibited internal phase-boundary cracks. Examples of these cracks are shown in Fig. A.15. Typically, these cracks were found in regions of fine microstructure adjacent to weld-pass fusion lines as shown in Fig. A.15a. Other features exhibited by the creep-rupture specimens were highly "rumpled" surfaces parallel to the specimen axis (especially for those specimens tested at 650°C) and ellipsoidally deformed cross sections with the minor axis parallel to the general solidification direction, as shown in Fig. A.16.

The metallographic and fractographic examinations of the creep-fatigue and creep-rupture specimens also revealed the presence of numerous inclusions embedded in the austenitic matrix and on the phase-boundary interfaces. One of the larger inclusions observed is shown in Fig. A.17. An energy-dispersive X-ray analysis of several inclusions indicated that they were rich in silicon and manganese.

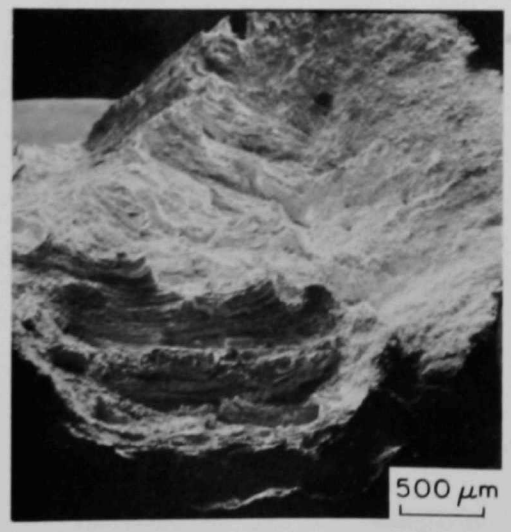

Fig. A.12

Scanning-electron Macrograph of Surface of Specimen 775-L3. ANL Neg. No. 306-77-637.

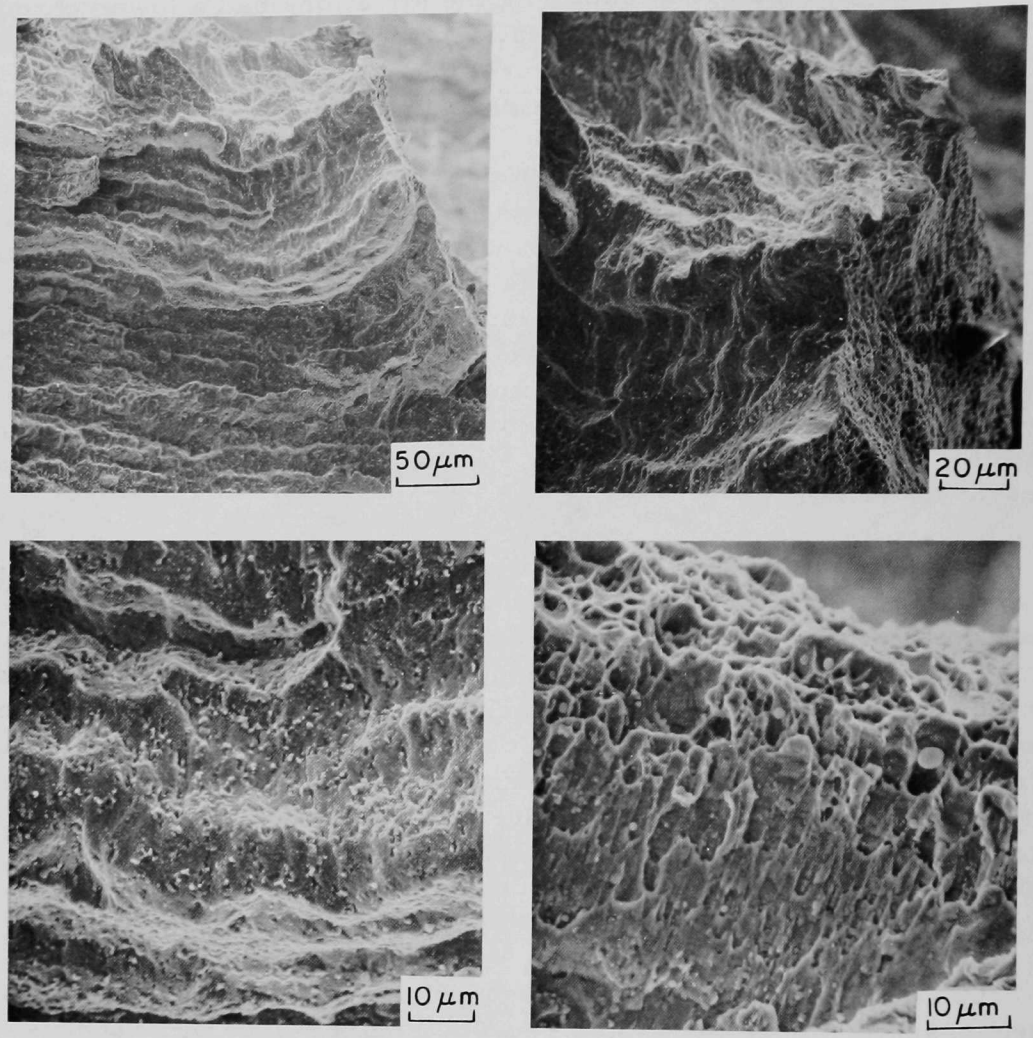

Fig. A.13. Fractographs of Specimen 775-L3. ANL Neg. Nos. 306-77-629 and 306-77-630.

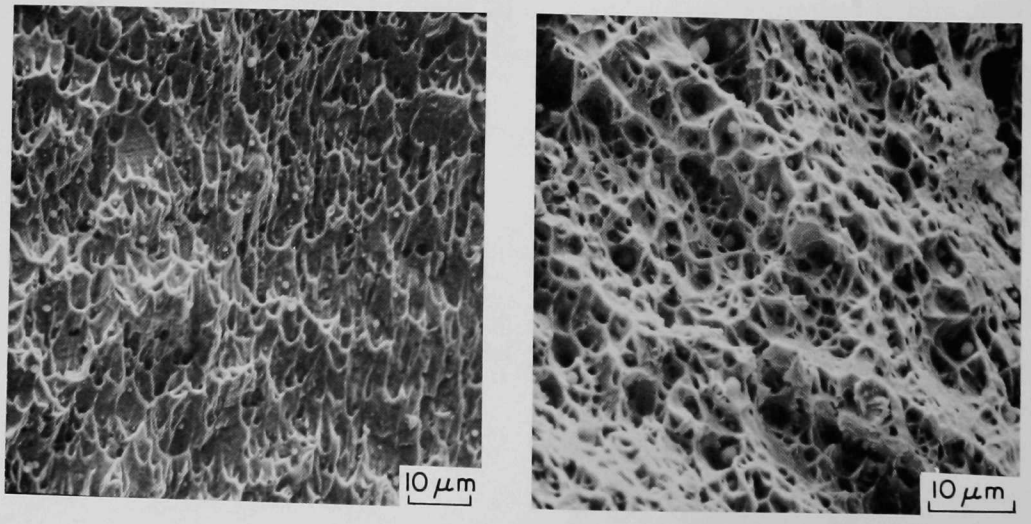

Fig. A.14. Fractographs of Specimens (a) 775-L1 and (b) 775-L14. ANL Neg. No. 306-77-645.

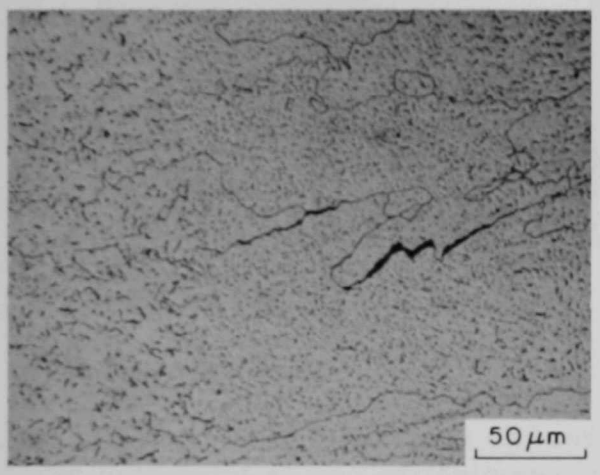

(a)

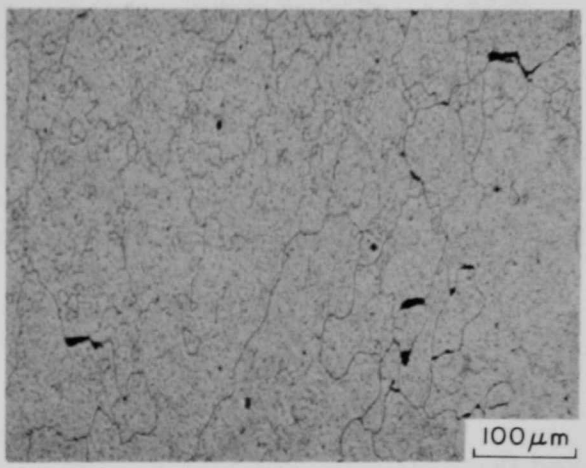

(b)

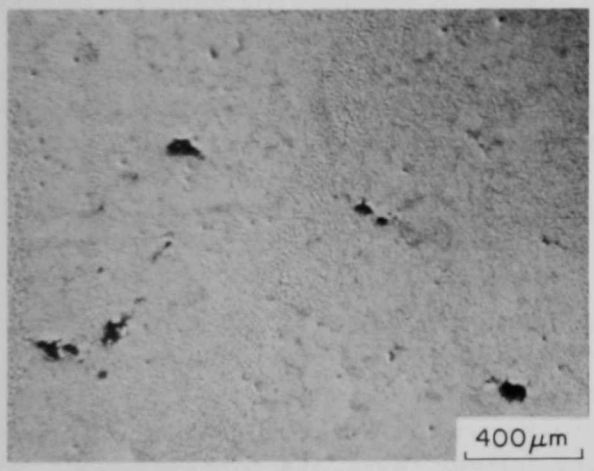

(c)

Fig. A.15

Photomicrographs of Internal Damage in Specimens (a) 775-L9, (b) 775-L14, and (c) 775-L1. Oxalic acid. ANL Neg. No. 306-77-642.

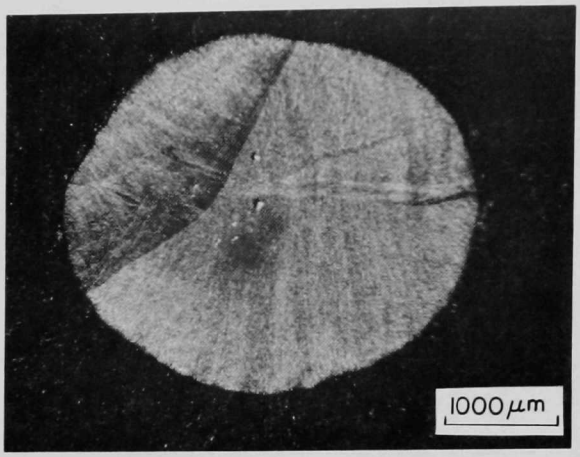

Fig. A.16. Macrograph of Cross Section of Specimen 775-L14. Oxalic acid. ANL Neg. No. 306-77-641.

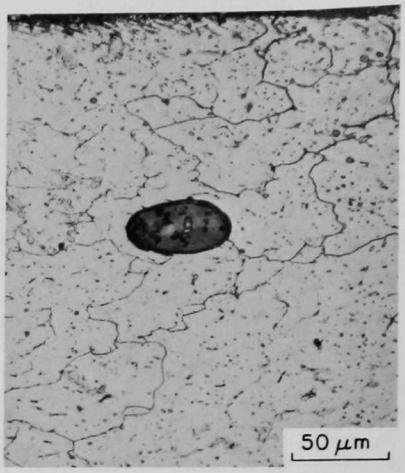

Fig. A.17. Photomicrograph of an Inclusion in Specimen 775-L14. Oxalic acid. ANL Neg. No. 306-77-639.

In summary, the difference between the creep-test results from ORNL and the creep-fatigue test results of this investigation can be attributed to different failure mechanisms. Failures associated with continuous cyclic straining are similar to transgranular cracking in wrought materials. In tests containing a hold time at peak tensile strain, the failure mechanism becomes a mixture of matrix and interphase cracking, with the latter more pronounced at longer hold times. The failure mechanism for creep tests appears to be primarily interphase separation, with some areas showing microvoid coalescence. Thus an austenitic weld metal with poor creep-rupture properties will not necessarily exhibit poor creep-fatigue resistance as observed in wrought materials.

Moreover, the results of the metallographic and fractographic analysis discussed here suggest the following conclusions regarding the results of continuous-cycling and creep-fatigue tests on weld-deposited Type 16-8-2 and wrought Type 316 stainless steels. When both materials exhibit similar fracture mechanisms, as in continuous-cycling fatigue tests, the longer lives obtained for the weld metal can be attributed to its finer microstructure. Similarly, when hold times at peak tensile strain are introduced in each cycle, the wrought material, with a relatively coarse microstructure, tends to fracture intergranularly while the weld metal retains a high resistance to interphase cracking and therefore has longer fatigue lives.

ACKNOWLEDGMENTS

I am grateful for the help of J. C. Tezak, C. F. Peterson, and M. D. Gorman in the test program and data reduction. Special appreciation is due to W. F. Burke for his assistance in resolving the many experimental difficulties encountered in this investigation. Appreciation is also due to R. T. King of Oak Ridge National Laboratory for aid in procuring the material and for helpful discussions on the properties of weld metals. I also wish to thank D. R. Diercks and R. W. Weeks for their support and encouragement.

REFERENCES

1. O. R. Carpenter and R. D. Wylie, Met. Prog. *70*(5), 65-73 (Nov 1956).
2. A. L. Ward, J. E. Irvin, L. D. Blackburn, G. M. Slaughter, G. M. Goodwin, and N. C. Cole, *Preparation, Characterization, and Testing of Austenitic Stainless Steel Weldments,* Hanford Engineering Development Laboratory, HEDK-TME-71-118 (Aug 1971).
3. G. M. Goodwin, N. C. Cole, and G. M. Slaughter, Weld. J., Research Supplement *51*(9), 425s-429s (Oct 1972).
4. A. L. Ward, *Austenitic Stainless Steel Weld Materials--A Data Compilation and Review,* Hanford Engineering Development Laboratory, HEDL-TME-74-25 (May 1974).
5. R. T. King, N. C. Cole, R. G. Berggren, and G. M. Goodwin, "Properties and Structure of 16-8-2 Strainless Steel Weld Metal," *Second National Congress on Pressure Vessels & Piping,* San Francisco, June 23-27, 1975, ASME Publication No. 75-PVP-45.
6. R. T. King and D. P. Edmonds, in *Mechanical Properties Test Data for Structural Materials, Quarterly Progress Report for Period Ending April 30, 1976,* Oak Ridge National Laboratory, ORNL-5150, pp. 135-146.
7. A. L. Ward and L. D. Blackburn, J. Eng. Mater. Technol., Trans. ASME, Series H *98*(3), 213-220 (July 1976).
8. C. R. Brinkman, V. K. Sikka, and R. T. King, in *Mechanical Properties of LMFBR Primary Piping Materials,* Oak Ridge National Laboratory, ORNL-5199 (Nov 1976).
9. C. R. Brinkman and G. E. Korth, *Heat-to-heat Variations in the Fatigue and Creep-fatigue Behavior of AISI Type 304 Stainless Steel at 593°C,* J. Nucl. Mater. *48,* 293-306 (1973); also, Aerojet Nuclear Company, ANCR-1097 (May 1973).
10. D. R. Diercks and D. T. Raske, *Elevated-temperature, Strain-controlled Fatigue Data on Type 304 Stainless Steel: A compilation, Multiple Linear Regression Model, and Statistical Analysis,* ANL-76-95 (Dec 1976).
11. P. S. Maiya and S. Majumdar, in *Mechanical Properties Test Data for Structural Materials, Quarterly Progress Report for Period Ending October 31, 1976,* Oak Ridge National Laboratory, ORNL-5237, pp. 23-38.
12. C. R. Brinkman, G. E. Korth, and J. M. Beeston, *Comparison of the Fatigue and Creep-Fatigue Properties of Unirradiated and Irradiated Type 304 and 316 Stainless Steel at 593°C (1100°F),* Aeroject Nuclear Company, ANCR-1078 (Aug 1972).
13. R. W. Weeks, D. R. Diercks, and C. F. Cheng, *ANL Low-cycle Fatigue Studies--Program, Results, and Analysis,* ANL-8009 (Nov 1973).
14. T. Slot, R. H. Stentz, and J. T. Berling, in *Manual on Low Cycle Fatigue Testing,* ASTM STP 465, Am. Soc. Test. Mater., pp. 100-128 (1969).
15. JoDean Morrow, in *Internal Friction, Damping, and Cyclic Plasticity,* ASTM STP 378, Am. Soc. Test. Mater., pp. 45-87 (1965).

16. L. A. James, Weld. J., Research Supplement *52*(4), 173s-179s (April 1973).

17. R. Shahinian, H. H. Smith, and J. R. Hawthorne, Weld. J., Research Supplement *51*(11), 527s-532s (Nov 1972).

18. D. T. Raske and C. F. Cheng, *Fatigue Crack Propagation in Types 304 and 308 Stainless Steel at Elevated Temperatures*, Nucl. Technol. *34*(1), 101-110 (June 1977).

19. N. F. Fiore and D. R. Diercks, J. Eng. Mater. Technol., Trans. ASME, Series H *99*(1), pp. 29-35 (Jan 1977).

20. J. M. Beeston and C. R. Brinkman, in *Irradiation Effects on Structural Alloys for Nuclear Reactor Applications*, ASTM STP 484, Am. Soc. Test. Mater., 1970, pp. 419-450.

21. P. S. Maiya and D. E. Busch, Metall. Trans. A *6A*, 1761-1766 (Sept 1975).

22. D. T. Raske, *Section and Notch Size Effects in Fatigue*, University of Illinois T&AM Report No. 360, Urbana (Aug 1972).

23. R. W. Landgraf, JoDean Morrow, and T. Endo, J. Mater., JMLSA *4*(1), 176-188 (March 1969).

24. D. T. Raske and JoDean Morrow, in *Manual on Low Cycle Fatigue Testing*, ASTM STP 465, Am. Soc. Test. Mater., pp. 1-25 (1969).

25. C. E. Jaske, H. Mindlin, and J. S. Perrin, in *Cyclic Stress-Strain Behavior Analysis, Experimentation, and Failure Prediction*, ASTM STP 519, Am. Soc. Test. Mater., pp. 13-27 (1973).

26. B. R. Dewey, in *Mechanical Properties Test Data for Structural Materials, Quarterly Progress Report for Period Ending July 31, 1976*, Oak Ridge National Laboratory, ORNL-5200, pp. 149-154.

27. Personal communication, T. K. Roche, Oak Ridge National Laboratory, to D. T. Raske, Argonne National Laboratory (Feb 1977).

28. J. R. Griffiths, I. L. Mogford, and C. E. Richards, Met. Sci. J. *5*, 150-154 (1971).

Distribution of ANL-77-72

Internal:

J. A. Kyger
A. Amorosi
R. Avery
L. Burris
D. W. Cissel
S. A. Davis
B. R. T. Frost
D. C. Rardin
R. G. Staker
R. J. Teunis
C. E. Till
R. S. Zeno
C. E. Dickerman
H. K. Fauske
S. Fistedis
B. D. LaMar
J. F. Marchaterre
H. O. Monson
R. Sevy
P. R. Fields
D. C. Price
D. T. Raske (10)
M. D. Gorman
C. F. Peterson
J. C. Tezak
W. F. Burke
C. F. Cheng
R. W. Weeks
F. A. Nichols
L. T. Lloyd
M. F. Adams (2)
N. L. Peterson
J. F. Schumar
T. H. Blewitt
M. B. Brodsky
D. R. Diercks
F. Y. Fradin
A. G. Hins
T. F. Kassner
U. F. Kocks
L. A. Neimark
K. L. Merkle
M. H. Mueller
R. B. Poeppel
K. J. Reimann
R. W. Siegel
D. Stahl
H. R. Thresh
H. Wiedersich
A. B. Krisciunas
ANL Contract File
ANL Libraries (5)
TIS Files (6)

External

DOE-TIC, for distribution per UC-79h (249)
Manager, Chicago Operations Office
Chief, Chicago Patent Group
Director, DOE-RRT (2)
Director, Reactor Programs Div., CH
Director, CH-INEL
President, Argonne Universities Association
Materials Science Division Review Committee:
- G. S. Ansell, Rensselaer Polytechnic Inst.
- R. W. Balluffi, Cornell U.
- S. L. Cooper, U. Wisconsin
- S. Doniach, Stanford U.
- H. L. Falkenberry, Tennessee Valley Authority
- C. Laird, U. Pennsylvania
- D. Lazarus, U. Illinois
- M. T. Simnad, General Atomic
- A. R. C. Westwood, Martin Marietta Labs.

ARGONNE NATIONAL LAB WEST
3 4444 00011016 3